EasyChair Preprint

№ 6354

Aerodynamic Design and Performance Analysis of the Ultra-High Expansion Ratio Turbine for Trans-Media Engines

Siyu Wu, Jie Gao, Cheng Zhou and Weiliang Fu

August 23, 2021

Proceedings of Global Power and Propulsion Society
ISSN-Nr: 2504-4400
GPPS Xi'an21
18th – 20th October, 2021
www.gpps.global
GPPS-TC-2021-0125

Aerodynamic design and performance analysis of the ultra-high expansion ratio turbine for trans-media engines

Siyu Wu
College of Power and Energy Engineering,
Harbin Engineering University
wusiyu001@qq.com
Harbin, Heilongjiang, P.R.C

Jie Gao*
College of Power and Energy Engineering,
Harbin Engineering University
gaojie_d@hrbeu.edu.cn,
Harbin, Heilongjiang, P.R.C

Cheng Zhou
College of Power and Energy Engineering,
Harbin Engineering University
1325001817@qq.com

Weliang Fu
College of Power and Energy Engineering,
Harbin Engineering University
fuweil@hrbeu.edu.cn, Harbin, Heilongjiang, P.R.C

Abstract

In order to produce more specific work in trans-media engines, which features low-mass flow feeding systems, the flow loss of ultra-high expansion turbine with single stage need to be studied further. In this paper, the numerical method was used to carry out calculations for turbines in both air and underwater working conditions, and the flow fields inside the flow passage of ultra-high expansion ratio turbines are studied in detail. The results show that the power, efficiency and flow requirements of the engine in the air condition and underwater conditions can be met by changing the number of nozzles and the throat area while keeping the blades unchanged. In underwater working conditions, shock waves are formed obviously between one nozzle outlet and suction surfaces of three rotor blades, while in the air conditions, shock waves are only formed between one nozzle outlet and suction surface of two rotor blades . Therefore, overall, the efficiency in the underwater condition is significantly less than that in the air condition. In the both conditions, the gas in the blade passage corresponding to the circumferential gap between the two nozzles generates vortices due to mutual mixing, resulting in vortex losses.

Keywords: Trans-media engine, Ultra-high expansion ratio turbine, Shock wave, Aerodynamics

Introduction

The dynamic system of underwater vehicles has a decisive influence on its performance. Since long range and fast speed are the development trend of future underwater vehicles, thermal-power system engines have great advantages. For the production of underwater vehicles, most countries use the thermal propulsion system. Due to the volume requirements of the vehicle, the piston engine is only suitable for working in the case of low-power requirements. The turbine engine is used more and more widely, as a rotating machine, the vibration of the engine is small, which can meet the requirements of high-power vehicles. So turbine engine represents the development trend of future underwater vehicle power system [1-4].

The turbine adopted by the water-air medium aircraft has the advantages of small size and large power, which can meet the requirements of the aircraft in air and underwater conditions [5]. Wang [6] described the progress in computer technology and the development of computational fluid dynamics in recent years. The study of the flow inside the impeller is changed from the past experiments to the application of computational fluid dynamics, which can greatly improve the efficiency and save time resources.

Yi et al. [7] carried out numerical calculations on the flows in the moving blades of some partial inlet turbines, and found that there were many vortices in the flow passage, which would cause energy dissipation and increase the loss. Yi et al. [8] studied the complex internal flows of a turbine by calculating its flow field in variable working conditions, and found that the results were relatively close to the experimental data. Gas flow in some partial inlet turbines has no rules to follow, because the gas flowing around the blades is viscous, and a boundary layer will be formed around the blades. Changes in blade surface pressure will lead to secondary flows, vortexes and other flow phenomena, thus resulting in flow losses.

Guo et al. [9] carried out numerical simulation on pure impulse turbine, and carefully analyzed the temperature change, load change and loss change in the flow passage corresponding to the rotor blade of the nozzle. It was found that the higher the blade load, the lower the temperature, and the smaller the temperature gradient.

Liu et al. [10] carried out unsteady calculation for a single stage turbine with a large expansion ratio up to 30. It was found that the wake of the nozzle changed greatly along the radial direction, and there were various wave systems in the rotor blade passage. Chen et al. [11] used CFX to calculate torpedo turbine and analyzed rotor blade runner. It was found that oblique shock waves appeared at the trailing edge of rotor blade, forming swallowtail vortex.

Chen et al. [12-13] studied local inlet turbines and found that the distribution of static pressure along the circumferential direction was uneven, and the pressure distribution on the blade surface at different positions was also different. It is found that the total static efficiency of the re-entry turbine will increase after adjustment.

As seen, there was a lot of research in ultra-high expansion ratio turbine, but there is little research about the flow loss mechanism in trans-media engine. Therefore, it is necessary to analyze the complex internal flows of turbines used in trans-media engine.

In this paper, CFX, computational fluid software, is used to calculate the whole cycle of some partial inlet turbines in the air condition and under-water conditions, and analyze the flow phenomena of the flow passage inside the turbine in the inlet area and the load on the blades.

Numerical method

Nozzle calculation model

According to the total inlet temperature *T*, flow rate and expansion ratio, the isentropic velocity at the nozzle outlet can be obtained through formula (1):

$$v_1 = \sqrt{2h^*} \tag{1}$$

In formula (1),$h^*$is the isentropic enthalpy drop in the nozzle;v_1 is the ideal velocity of nozzle outlet.

Apply formula (2) to calculate the area:

$$\dot{m} = \rho v A \tag{2}$$

In formula (2), *A* is the area of nozzle inlet, outlet and throat; *v* is the velocity of inlet, outlet and throat; ρ is the gas density of nozzle inlet, outlet and throat.

$$l = \frac{d_1 - d_{\mathrm{cr}}}{2tan\left(\frac{\varphi}{2}\right)} \tag{3}$$

In formula (3), d_1 is the diameter of nozzle outlet; d_{cr} is the radius of the nozzle throat; $\varphi$is the tip cone Angle of the nozzle. The shape and size of the nozzle can be drawn through formula (1) ~ (3), as shown in Fig. 1.

Since this turbine stage is a single-stage turbine, the enthalpy drop is very large. In addition, when the gas flows out of the nozzle outlet after expansion in the nozzle, the speed reaches the supersonic, and the speed is used to push the turbine blades to do work.

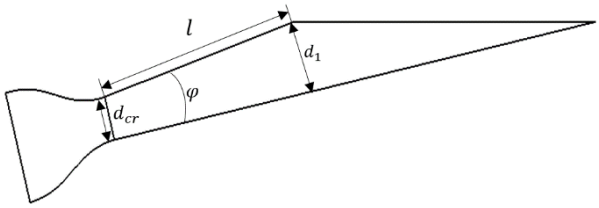

Figure 1. Nozzle model

Turbine blade calculation model

Because the fuel carried by the aircraft is certain, the mass flow through the turbine is very small, partial inlet turbines are widely used. Considering the height of turbine blades is also relatively small, it is very complicated to make complex blade shapes on short blades. Therefore, for the convenience of design and manufacturing, the blade profile is drawn by lines and circles, as shown in Fig. 2.

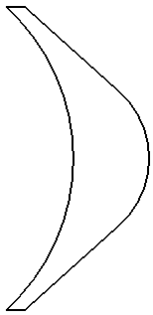

Figure 2. The turbine rotor blade profile model

(a) Calculation domain model in the air condition

(b) Computational domain model in the underwater condition

Figure 3. Turbine computational domain model

Figure 3 shows the computational domain model, to meet the power requirements of the aircraft both in air and underwater conditions. Therefore, when the vehicle is in the air condition, the stator blade adopts the form of four nozzles, and when the vehicle is in the underwater condition, the stator blade adopts the form of two nozzles.

The numerical simulation

Because the nozzle is not in a form of circumferential symmetrical distribution structures, it is necessary to conduct a full cycle numerical calculation on the turbine. In order to achieve better data transfer between rotor and stator, a ring of transition was connected at the nozzle outlet and the frozen rotor method was adopted for data transfer between rotor and stator. In this paper, the computational fluid software ANSYS CFX 17.0 is used for numerical calculation of the turbine. The turbulence model adopts k-w, and the near-wall surface adopts Automatic for wall surface treatment. The nozzle inlet is given the total inlet temperature and total pressure, the moving blade outlet is given the static pressure, and the wall surface is given the adiabatic and non-slip boundary conditions

Computational grids

In ANSYS ICEM, hexahedral structured grid division was conducted for nozzles and transition rings. AutoGrid5 in NUMECA was used to conduct structured grid division for turbine rotor blades, as shown in Fig. 4.

In order to more accurately understand the gas flow through the wall, changes in the velocity, temperature, pressure and other parameters need to refine the nozzle wall and rotor blade mesh. As the full-cycle calculation is adopted, the number of meshes of four nozzles in the air condition is 2.91 million, the number of meshes of two underwater nozzles is 1.46 million, and the number of meshes of the flow passage part of a single rotor blade is 360,000. Therefore, the total number of meshes in the calculation domain in air working condition is 26 million, while that in the calculation domain in underwater working condition is 24.5 million.

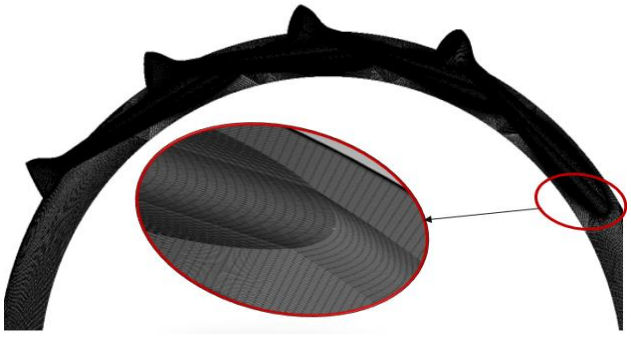

(a)Four nozzles grid in air condition

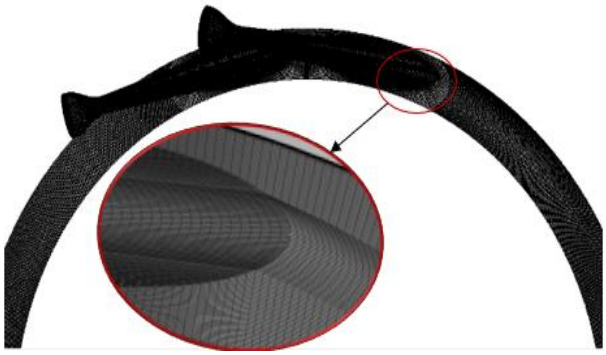

(b) Two nozzles grid in underwater condition

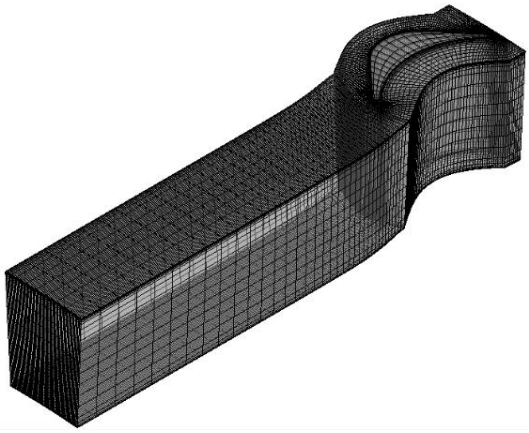

(c) Single rotor blade flow through part of the grid

Figure 4. Calculation grid of turbine rotor and nozzle

Results and discussion

Since the outlet of the nozzle is obliquely cut, when the gas flow just enters the rotor blade, the pressure and velocity of the gas are irregular. Moreover, in order to meet the requirements of the aircraft in the air and underwater conditions, the number of nozzles is different dependent on the boundary conditions. Obviously, the gas flow at the nozzle outlet is different in these two working conditions. So it is necessary to understand the flow mechanism of the rotor blade passage in the air inlet area in detail when the gas flow is in the air condition and the underwater working condition. Fig. 5 shows the Mach number contours at the middle diameter of the rotor impeller in the both conditions.

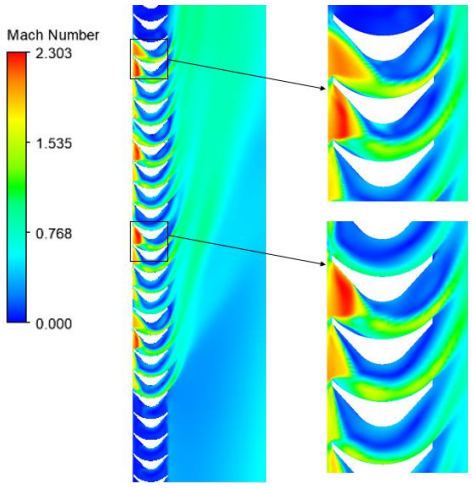

(a) Mach number at 50% of blade height in the air condition

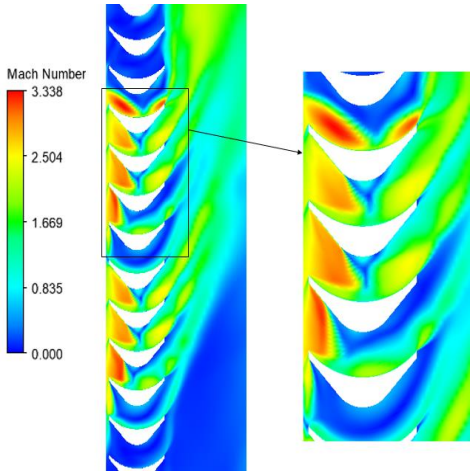

(b) Mach number at 50% of blade height in the underwater condition

Figure 5. Mach number contours at the height of 50% of the blade

It can be seen from Fig. 5 that when the turbine is in the air condition, the gas flow ejected from the nozzle is supersonic with a Mach number of 1.7 when it just enters the rotor blade passage. The gas flow will accelerate on the suction side and reach the maximum Mach number at the position of 25% of the axial chord length. The maximum value is 2.30 and a shock wave is formed. Downstream the shock wave, the gas Mach number and velocities will decrease. Moreover, shock waves cause the boundary layer separation on the suction surface, thus increasing the flow loss. When the gas flows through the outlet of the blade passage, the velocity on the pressure side will increase, and the Mach number will be higher than that in the middle of the passage, about 1.2. When the gas flows out of the trailing edge of the blade, the velocity decreases and becomes subsonic. When the turbine is in underwater condition, the Mach number at the inlet of the rotor blade corresponding to the nozzle outlet reaches 2, and the Mach number at the position of 30%-40% of the axial chord length reaches the maximum value, which is close to 3.338. It is obvious that the maximum Mach number in the blade passage is larger in the underwater condition than that in the air condition, and a large part of the gas flow in the blade passage corresponding to the nozzle outlet is supersonic in the underwater condition.

This part of gas flow is basically filled with the entire blade passage, and the Mach number is mostly above 1.6. However, in the air condition, the gas flow in the blade passage corresponding to the nozzle outlet only has a high Mach number before the position of the axial chord length of 40%. The gas velocity of the rest is obviously lower than that in the underwater condition, and one nozzle outlet obviously cause shock waves on the suction surfaces of the three rotor blades. In the air condition, however, only two shock waves are apparent at the suction side. When the gas flows through the trailing edge of the blade, the gas Mach number near the pressure surface reaches the maximum value of 2, which is obviously much larger than that in air condition. Therefore, the kinetic energy at the turbine outlet in the underwater condition is significantly greater than that in the air condition. As this part of residual quick moving energy is not fully utilized by the turbine, it is lost. It can be seen that for the blade passage corresponding to the nozzle, the flow loss is much greater when the nozzle is in underwater condition than when it is in the air condition. In order to make full use of the kinetic energy at the outlet of the rotor blade, the gas flow at the outlet of the rotor blade can be used in the next turbine.

As can be seen from the analysis in Fig. 5, the velocity of gas flow in the rotor blade passage will change greatly. Even if the gas flows in the same inlet area, the flow state of the gas in each passage is different, leading to different surface pressures of the blades in the inlet area. Since the surface pressure of the blade pushes the blade to do work, the surface pressure of the blade corresponding to the inlet area determines the turbine's power capacity. Therefore, it is necessary to study the surface pressure of the blade corresponding to the inlet area and the non-inlet area to determine which blades have a great influence on the work.

Rotor flow field and blade load in the air condition

The air condition rotors were numbered from 1-64 in the clockwise direction and the blue blade was numbered as no. 1, as shown in Fig. 6.

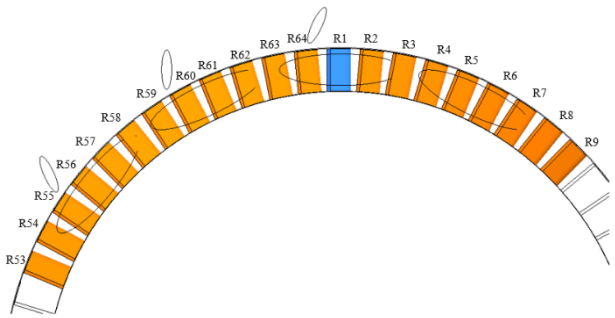

Figure 6. Naming of each blade in the air condition

Fig. 7 shows that the gas at the blade root in the flow passage between R1 and R2 flows along the blade from the blade root to the blade tip and forms vortexes. This is mainly because the circular movement of the blade causes the gas at the blade root to flow along the blade root to the blade tip, leading to an increase in friction loss and an increase in flow loss.

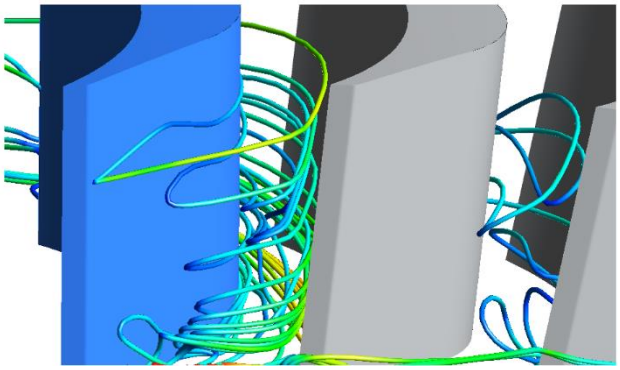

Figure 7. Vortices in the passage between R1 and R2 blades in the air condition

In order to prevent the collision between the rotor blade and the wall surface, it is necessary to keep a radial clearance at the blade tip. Since there is a pressure difference between the blade basin and the blade back, it is obvious that the gas at the blade tip flows from the pressure to the suction surfaces, and then clearance leakage vortexes were formed. From Fig. 8, it is obvious that gas flows from the pressure surface to the suction surface occur at the blade tips of R2 and R3, and clearance vortices are formed at the trailing edge of the blade.

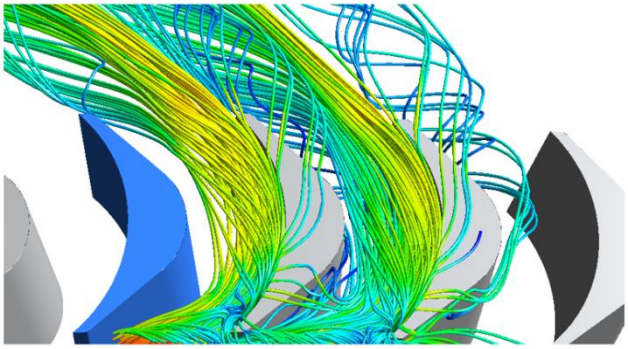

Figure 8. Schematic diagram of blade clearance leakage in the air condition

Since the two nozzles are not closely connected, there is a certain gap. Figure 6 shows that blade R63 is at the gap between adjacent nozzles. It can be seen from Fig. 9 that vortices will be generated in the flow passages of blades R63 and R64 at the gap between two nozzles. This is mainly because the gas in the flow passage is provided by two nozzles. The gases coming out of the two nozzles mix with each other and eventually tend to homogenize. In the process of mixing, vortexes are generated and vortex losses are caused.

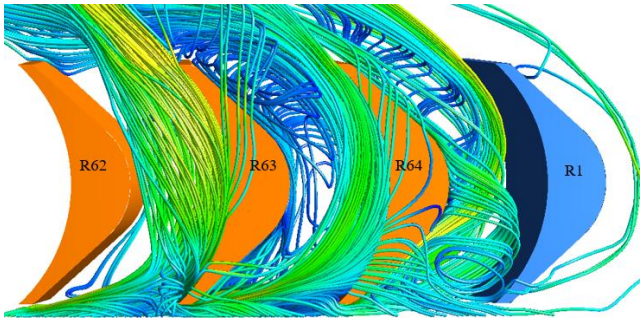

Figure 9. Internal streamline of the rotor blade passage corresponding to the circumferential gap between two adjacent nozzles in the air condition

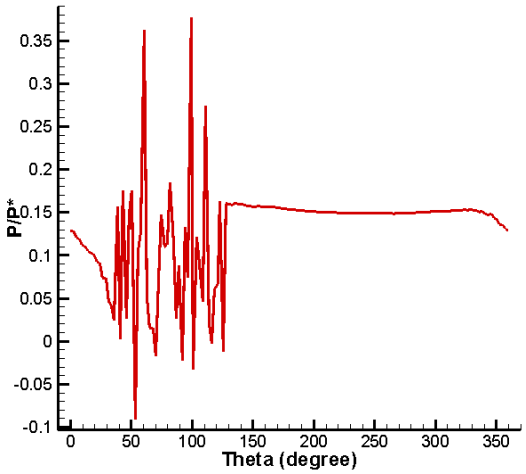

Figure 10. Circumferential distribution of dimensionless static pressure along the rotor inlet at 50% of the blade height in the air condition

As can be seen from Fig. 10, the static pressure at the inlet of the rotor blade varies unevenly along the circumference. The static pressure changes dramatically in the inlet area. And, in the non-inlet region the static pressure changes very little.

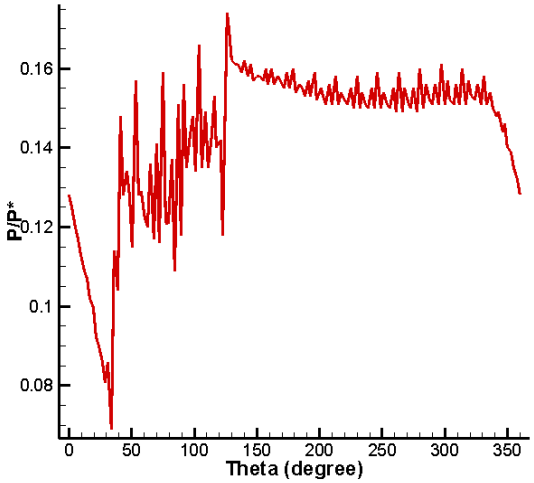

Figure 11. Circumferential distribution of dimensionless static pressure along the rotor outlet at 50% of the blade height in the air condition

As can be seen from Fig. 11, the static pressure at the rotor blade outlet varies greatly along the circumference, and the static pressure at the rotor blade outlet corresponding to the nozzle changes most significantly. The static pressure is the greatest when the rotor blade rotates out of the intake area, while the static pressure changes are relatively small in the rest parts. Compared with the static pressure at the inlet of the rotor blade, the static pressure at the outlet varies less.

The dimensionless pressure coefficient is defined as shown in formula (4), where P is the gas flow static pressure, P_1 is the relative static pressure at the outlet of the rotor blade, and P^* is the relative total gas pressure at the inlet of the rotor blade. The dimensionless value C_P was used as the ordinate and the relative axial chord length position was used as the abscissa to analyze the surface pressure on the blade.

$$C_P = \frac{P - P_1}{P^* - P_1} \tag{4}$$

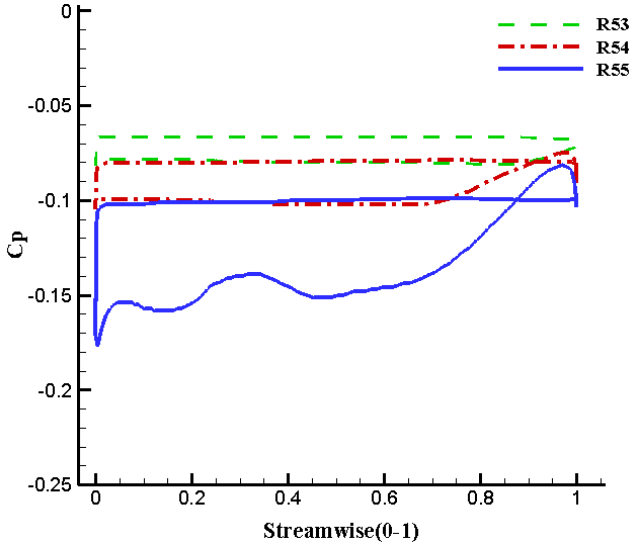

Figure 12. Pressure coefficient distribution of blade 53-55 at the height of 50% blade in the air condition

Since blades R53 and R54 are in the non-inlet region and blade R55 is in the inlet region, Fig. 12 can represent the load on the blades when they start to enter the inlet region. It can be seen from Fig. 12 that the pressure difference between the pressure surface and the suction surface of R53 and R54 is very small. Basically negligible, the blade's ability to do work is relatively weak. The pressure difference between the pressure surface and the suction surface of R55 blade is larger than that between R53 and R54. And before the position of 82% relative to the chord length, the pressure surface pressure is greater than the suction surface pressure. The load on the blade is large and the power to the blade is strong.

The inlet area of the rotor blade corresponding to the nozzle outlet is the main work area of the blade, and the blades of R59-R63 are all in the inlet area. Figure 13 shows the distribution of surface pressure coefficients at the middle diameter of blades R59-R63. It can be seen from Fig. 13 that the lateral pressure coefficients of suction surfaces of blades R59, R61,

R62 and R63 change little and gently. R60 blade suction surface near the blade leading edge side pressure there will be a rising trend, which may be caused by shock wave on the suction surface side, blade R59 before 30% relative chord length, the lateral pressure in the pressure side showed a trend of decline after leveled off, this may be due to R59 leaves will soon turn out the mainstream of the adjacent before a nozzle area. Before the position of blade R62 and blade R63 at the position of 20% relative chord length, the lateral pressure on the pressure surface shows a significant downward trend, which may be caused by the fact that these two blades are about to turn out of the main flow channel of the corresponding nozzle. The difference between the pressure side of the blade R60 and R61 and the suction side pressure is relatively large, and the area enclosed by the pressure line represents the amount of work done by the blade. The area enclosed by the pressure line R60 and R61 is larger than that of other blades. So these two blades have the maximum load and strong power capacity.

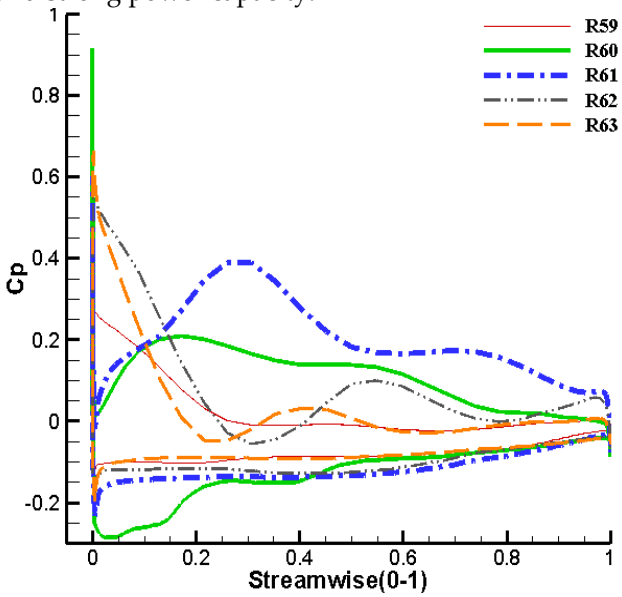

Figure 13. Surface pressure coefficient curve of blade 59-63 at the height of 50% blade in the air condition

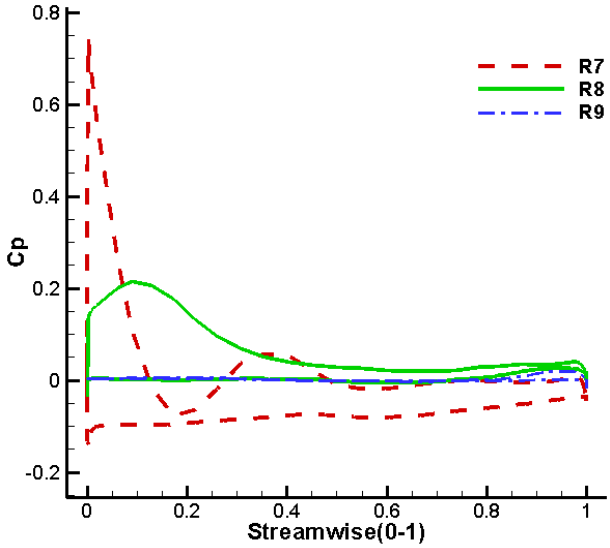

Figure 14. Surface pressure coefficient curve of blade 7-9 at the height of 50% blade in the air condition

Blades R7, R8 and R9 are the transition blades from the inlet area to the non-inlet area. As can be seen from Fig. 14, the pressure difference between the suction surface and the pressure surface of blade R7 and R8 is relatively large and the blade load is high, so the two blades have strong power capacity. The pressure difference between the pressure surface and suction surface in the non-inlet area of blade R9 is very small and no work is done. Before blade R7 reaches the position of 20% relative chord length, the lateral pressure on the pressure surface will decrease obviously. And the pressure difference between the pressure surface and the suction surface of the R8 blade is the largest at the position of 10% relative chord length. This is mainly caused by the fact that these two blades are about to turn out of the main flow channel corresponding to the nozzle outlet.

Rotor flow field and blade load in underwater condition

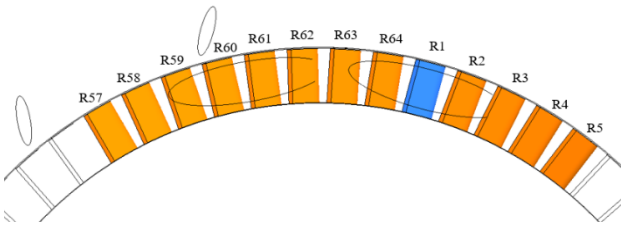

Figure 15. Naming of each blade in the underwater condition

According to Fig. 15, the moving blade in the underwater working condition is numbered from 1-64 clockwise, with the blue blade no. 1. R57, R58 and R59 are in the transition area from the non-inlet area to the inlet area. R59, R60, R61, R62 and R63 are in the inlet region, and R3, R4 and R5 are in the transition section from the inlet region to the non-inlet region.

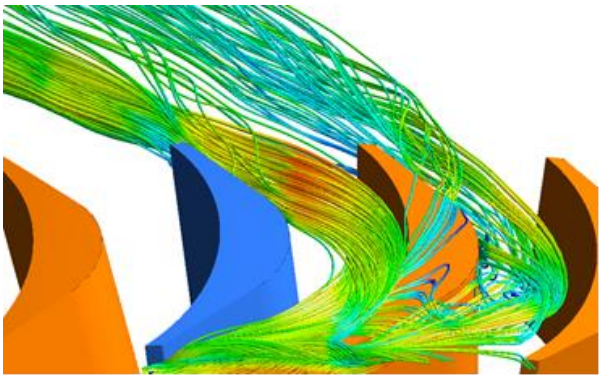

Figure 16. Blade clearance leakage of R2 in the underwater condition

Figure 16 shows that when the turbine is in water, the gas at the outlet of the nozzle will move towards the pressure surface at the tip of blade R2 by suction, and then roll into a vortex-clearance leakage vortex at the trailing edge of the blade. This is similar to the air condition, which will cause flow loss.

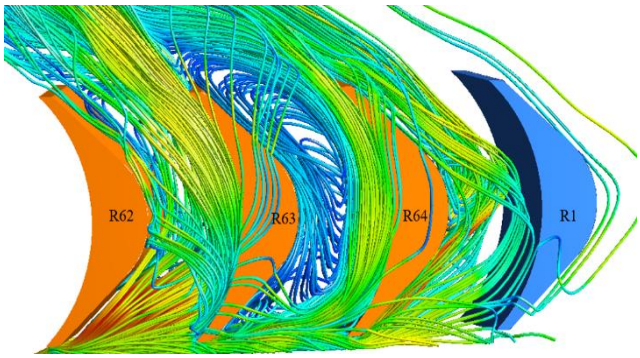

Figure 17. The streamline of the moving blade passage at the clearance between two adjacent nozzles in the underwater condition

When the turbine is in water, it can be seen from Fig. 15 that blade R63 is at the gap between adjacent nozzles. As can be seen from Fig. 17, a very significant vortex is generated in the blade passage between R63 and R64.This phenomenon also occurs in the air condition, which is mainly caused by the mixing of the gas at the outlet of the front and rear nozzles, resulting in severe eddy current loss. Therefore, it can be considered to reduce the gap between the two nozzles, or to overlap the outlet of the front and rear nozzles in a small part, so as to reduce the eddy current loss.

It can be seen from Fig. 18 that in the underwater condition, due to the decrease in the number of nozzles to two, the area with drastic changes in static pressure shrinks. However, the change of static pressure in the intake area is similar to that in the air condition.

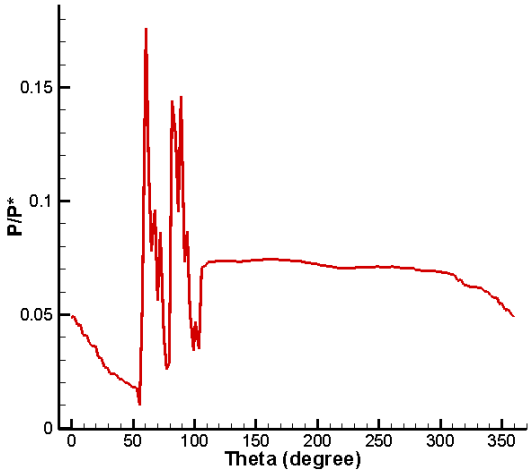

Figure 18. The dimensionless static pressure distribution along the circumference of 50% of the blade height at the inlet of the rotor blade in the

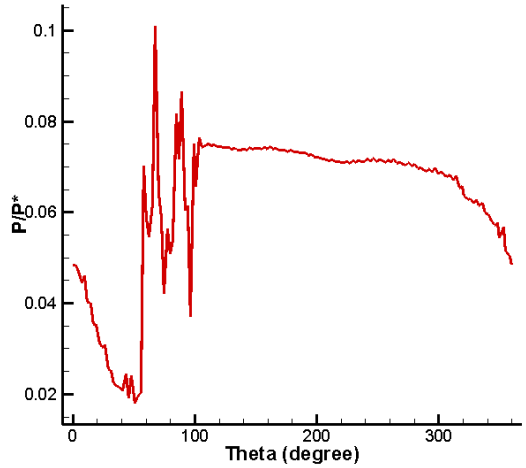

underwater condition

Figure 19. The dimensionless static pressure distribution along the circumference of 50% of the blade height at the outlet of the rotor blade in the underwater condition

As you can see in Fig. 19, the change in static pressure in the circumference direction is still large. As the number of nozzles decreases, the area at the outlet where the static pressure changes dramatically shrinks. And the average static pressure decreases compared to the inlet. This is mainly caused by the mixing of gas in the blade flow passage corresponding to the inlet area, so that the gas becomes more uniform.

Figure 20 shows that the pressure difference between the suction surface and the pressure surface of R57 and R58 is small with poor work capacity. R59 is in the inlet area at the beginning, and the pressure difference between the pressure surface and the suction surface is large, which is similar to the air condition. When the blade enters the inlet area at the beginning, the load on the blade will increase

suddenly, and the power capacity will become stronger suddenly.

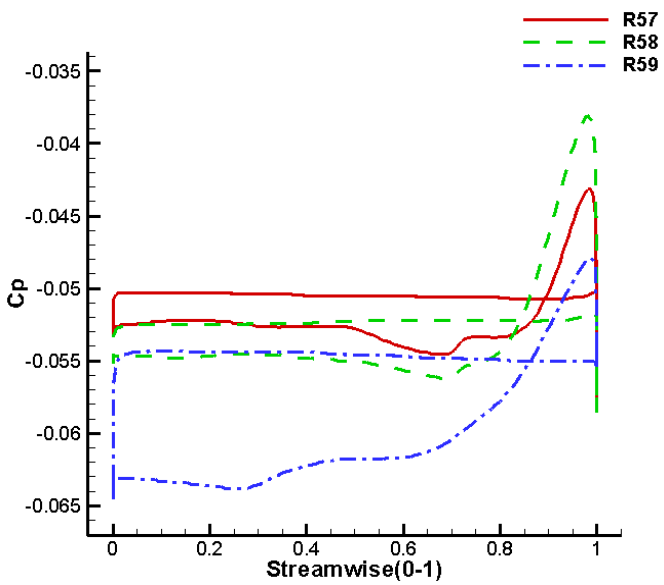

Figure 20. The surface pressure coefficient distribution at the middle diameter of blade R57 to R59 in the underwater condition

It can be seen from Fig. 21 that the pressure difference between the suction surface and the pressure surface of the four blades, R60, R61, R62 and R63, is large, so the four blades have strong work capacity. The pressure difference between the suction surface and the pressure surface of blade R59 is very small. Compared with that of blade R60, R61, R62 and R63 which are completely in the inlet area, they bear fewer loads. For nozzle exit of the inlet area in figure 21, besides blade R59 and R63 leaf R60, R61, R62 position in 60% axial chord length relative accessories differential pressure between suction surface and pressure surface will reach the maximum, and in the condition of the air condition, before the 30% relative axial chord length between pressure side and suction side pressure differential pressure will be maximum.

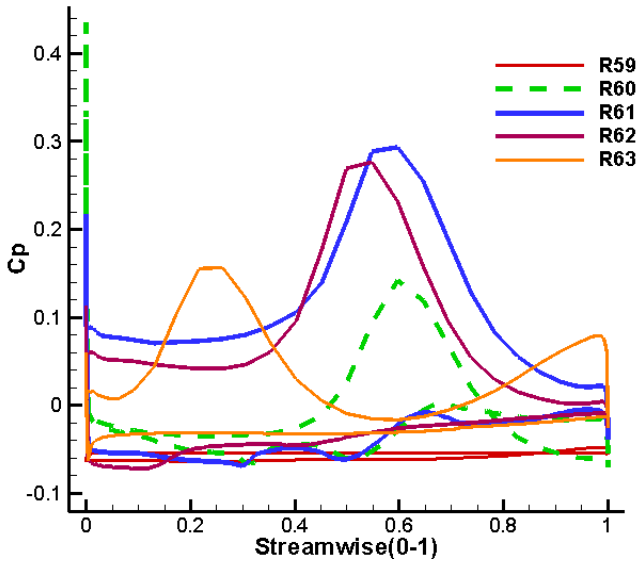

Figure 21. The surface pressure coefficient distribution at the middle diameter of blade R59 to R63 in the underwater condition

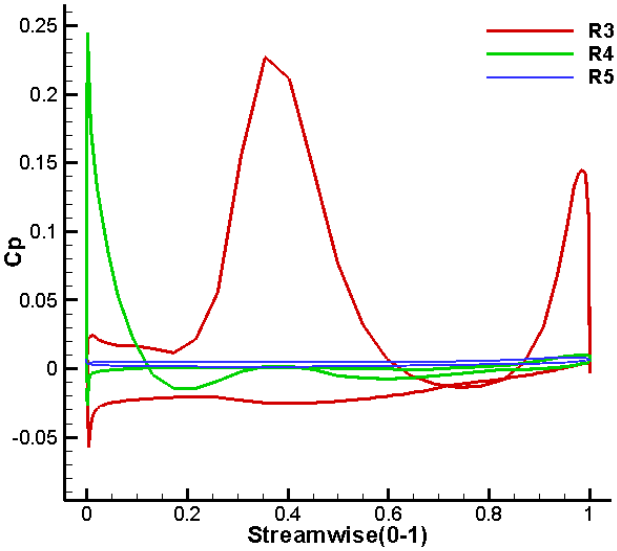

Figure 22. The surface pressure coefficient distribution from R3 to R5 at the median diameter of the blade in the underwater condition

Blade R3, R4 and R5 are in the transition section from the inlet area to the non-inlet area. It can be seen from Fig. 22 that the blade load of R3 is higher than that of R4 and R5, and the amount of work done by gas to the blade is the highest. R5 is basically in the non-inlet area, the pressure difference between the pressure surface and the suction surface is basically zero, and the blade load is very low.

Conclusions

(1) In the condition that the rotor blades remain unchanged, the number of nozzles and the throat

area can be changed to meet the requirements of power, efficiency and flow in the air and underwater working conditions of the engine.

(2) In underwater working conditions, one nozzle outlet will obviously cause shock waves on the suction surfaces of three moving blades, while in the air, it will only cause shock waves on the suction surfaces of two moving blades. The fundamental reason of this phenomenon is that the total inlet pressure of nozzle in underwater working condition is obviously higher than that in air working condition. This will cause residual velocity loss, so the flow loss of the turbine in the underwater working condition is more than that in the air working condition. Therefore, overall, the efficiency of underwater conditions is significantly less efficient than that of air conditions.

(3) Since the adjacent two nozzles are not closely connected, there is a certain clearance, and vortices will be generated in the blade passage at the clearance of the two nozzles, regardless of the air condition or the underwater condition. This is mainly because the gas in the flow passage is provided by two nozzles, and the gas coming out of the two nozzles will mix with each other, and vortexes will be generated in the process of change, resulting in eddy loss. Therefore, it can be considered to reduce the gap between the adjacent two nozzles, or to overlap the outlet of the front and rear two nozzles in a small part, so as to reduce the eddy current loss.

(4) The distribution law of pressure difference between suction surface and pressure surface of the blade at the air inlet area in air condition is obviously different from that in water condition. When the blade is in water, the pressure difference between the suction surface and the pressure surface will reach the maximum value near the position of 60% relative to the axial chord length. In the air condition, the maximum pressure difference between the pressure surface and the suction surface pressure occurs before the position of 30% relative to the axial chord length.

(5) Because a radial clearance is required at the blade tip, gas flowing from the pressure to the suction surface at the blade tip will be generated in the action of pressure difference, and then clearance vortexes will be formed, which will cause clearance leakage loss and affect turbine efficiency.

Nomenclature

h^*	isentropic enthalpy drop in the nozzle, kJ
v_1	ideal velocity of nozzle outlet, m/s
A	the area of nozzle inlet and outlet and throat, m^2
v	the velocity of inlet and outlet and throat, m/s
ρ	the gas density of nozzle inlet and outlet and throat, kg/s
d_1	the diameter of nozzle outlet, m
d_{cr}	the radius of the nozzle throat, m
φ	the tip cone Angle of the nozzle, deg
C_P	static pressure coefficient
P	Pressure, MPa
$\frac{P}{P^*}$	ratio of local static pressure to inlet relative total pressure

Acknowledgments

This work has been supported by the National Natural Science Foundation of China (Grant No. 51979052, 51779051) and the Fundamental Research Funds for the Central Universities (No. 307202CFT0304), which are gratefully acknowledged.

References

[1] B Chen, P F Zhang, K Guo, Review of the development in torpedo thermal power technologies. Journal of Propulsion Technology, vol. 32, no. 3, pp.447-450, 2011.

[2] S Z Wang, Z H Zhang, Y C Li, The Development of the Torpedo Thermal Power Engine and the Selection of the Engine Model. *Torpedo Technology*, vol.10, no.2, pp.5-9, 2002.

[3] Z W Zha, A Summary of Development in Torpedo Power Technologies. *Torpedo Technology*, vol.13, no.1, pp.1-4, 2005.

[4] M Lai, G Y Qi, P F Zhu, Research on the development of foreign torpedo power system. *Ship Science and Technology*, vol. 36, no.8, pp.154-157, 2014.

[5] Z W Zha, X F Shi, Z B Qian, Technique of Torpedo Thermal Power. Beijing: National Defense Industry Press, 2006.

[6] F J Wang, Computational Fluid Dynamics Analysis. Beijing: Tsinghua University Press, 2004.

[7] J B Yi, W B Zhao, H C Shi, et al. Numerical Simulation on Inner Flow Field of Gas Turbine with Partial Inlet Flow. *Torpedo Technology*, vol.18, no.6, pp.456-460, 2010.

[8] J B Yi, J P Qian, C P Dong, et al. Numerical Investigation on Turbine flow field and performance of underwater vehicle. *Torpedo Technology*, vol.17,no.4, pp.61-66,2009.

[9] Z Y Guo, H Cao, W B Zhao, Numerical Simulation of Supersonic Flow Field in Rotor Blade Cascade for Impulse Torpedo Turbine. *Torpedo Technology*, vol.21, no.1, pp.43-47, 2013.

[10] G T Liu, H Y Huang, X F Wang, et al. 3D Unsteady Numerical Investigation on Flow Field of Large Pressure Ratio Turbine. *Turbine Technology*, vol.54, no.6, pp.425-428, 2012.

[11] G Chen, J B Yi, H C Shi, Numerical Simulation of Torpedo Turbine Flow Passage Field and Performance Using ANSYS CFX. *Torpedo Technology*, vol.20, no.6, pp.285-294,2012.

[12] D Y Chen, J Z Zhong, J A Han, Numerical Investigation of the Non-uniform Flow Field for a High Loaded Partial Admission Turbine. *Journal of Engineering Thermophysics*,vol.37, no. 12, pp.2549-2556, 2016.

[13] D Y Chen, J Z Zhong, J A Han, Effect of inlet arcs adjustment on double-inlet re-entry turbine performance. *Journal of Dalian Maritime University*, vol.44, no.2, pp.74-80, 2018.3